Italian Association of Aeronautics and Astronautics
XXV International Congress
9-12 September 2019 | Rome, Italy

ORBITAL RESONANCE ANALYSIS IN MONTE CARLO SIMULATIONS FOR PLANETARY PROTECTION AND DEFENCE

Alessandro Masat[1,2*], Matteo Romano[1], Camilla Colombo[1]

[1*]Politecnico di Milano, DAER Dipartimento di Scienze e Tecnologie Aerospaziali, Politecnico di Milano, Via La Masa 34, 20156 Milano - Italy

[2]KTH Royal Institute of Technology, Brinellvägen 8, SE-100 44 Stockholm – Sweden

[1,2*]emails: alessandro.masat@mail.polimi.it, masat@kth.se
[1]email: matteo1.romano@polimi.it
[1]email: camilla.colombo@polimi.it

ABSTRACT

The study of close approaches and resonant returns features several applications, from monitoring near-Earth asteroids to the fulfilment of planetary protection requirements when injecting end-of-life spacecrafts into deep space orbits. Such studies are often performed using the b-plane, a reference frame where resonant returns are identified by circles, each representing a unique phasing condition.

The concept of resonant circle is here extended becoming a belt-shaped locus of points, to consider also quasi-resonant returns as threatening ones. The current theory is extended from the single body case to the analysis of a cloud of bodies all in a single b-plane representation, by modifying the initial circular shape to obtain a set of elliptical belts that match the simulated resonances.

Each simulation is built on high precision orbital propagations, including general relativity effects in the N-body dynamics with a validated, self-defined and efficient method, which is mentioned and applied.
The presented results highlight possible analytical developments to extend the original theory to Monte Carlo analyses of threatening near Earth asteroids, by studying a cloud generated from the uncertainties on nominal velocity and position, and designing end-of-life manoeuvres requiring, under a certain confidence level, such spacecraft to not be injected into a resonant trajectory.

Keywords: B-plane, Resonance, Resonant belts, Close approach.

1 INTRODUCTION

The problem of orbital resonances is meaningful in planetary protection and defence contexts, becoming particularly important when designing either end-of-life manoeuvres or asteroid deflection missions. It is crucial to make sure under a high confidence level that the small bodies under analysis are injected in a proper interplanetary orbit, such that they will not dangerously approach any planet or relevant body in future epochs. To support this last statement, a remarkable example is brought by the European Space Agency's planetary protection

requirements [1], which requires to design interplanetary injections so that, under a 99% confidence level, an uncontrollable upper stage after performing the manoeuvre does not impact with any planet, over 100 years after the injection itself.

To reach such high confidence levels high precision numerical simulations are required. It is of common knowledge [2] that in orbital motion a small error propagates and increases in time, with sudden steep growths every time that a fly-by occurs. In this regard, a complete N-body propagation considering gravitational forces coming from all the Solar System's planet may not be accurate enough, particularly if the propagation is to be carried out many years forward in time. Among the common orbital perturbations general relativity effects must be considered as well, even if strong gravitational sources are not remarkably close to the simulated body and especially if close approaches are present, to reach a propagation precision that basically matches SPICE ephemerides data [3].

Despite such a complete physical model features incomparable accuracy and reliability, the computational cost remains high for Monte Carlo simulations, where the motion of thousands of bodies is propagated and moreover the propagation results need to be post-processed to extrapolate relevant information about resonances. There exists then the need to seek for reliable analytical tools to study them, in order to obtain reliable predictions even without performing complete high precision simulations. The propagations may be carried out in such a way that they run just until the close approach is experienced, switching then the analysis into an analytical one, which provides remarkable information about future resonant close approaches or impacts.

This work makes a first step into this direction, trying to extend the already available resonance theory for 2-body motion to be modelling also other physical and formulation-related issues. The case studied is the resonance analysis of a cloud of points with gaussian distribution, generated from Apophis[1]' position and velocity, obtained from ephemerides data at the 1st January 2028. The nominal orbit already experiences a deep fly-by and, whether the resonance-check criterion presented in the development of this work is applied, the interplanetary trajectory after the close approach is classified as resonant. A cloud generated from such a condition would then allow to explore also other resonance regions in the b-plane without any peculiar assumption or loss of generality. Note that such a cloud could also have been built from an artificial initial point and would have had basically the same structure. Physical concepts highlighted by experimental results can therefore be considered as general as well.

2 TWO-BODY RESONANCE THEORETICAL CONCEPTS

The first theoretical tools to study orbital resonances have been developed in [4] and [5], whose concepts used in this work are reported in the current section. All the quantities involved are non-dimensional, with reference length to be the Astronomical Unit and reference time to be Earth's orbital period divided by 2π. The interplanetary reference frame considered in this work is the cartesian equatorial frame centred in the Solar System Barycentre (J2000), although, once studying resonances in the b-plane, any fixed cartesian interplanetary frame could be considered, provided that all the quantities involved are expressed consistently.

2.1 Planetocentric velocity and close encounter geometry

The planetocentric velocity $\boldsymbol{U} = (U_x, U_y, U_z), U = \|\boldsymbol{U}\|$ is the relative velocity between planet and small body [4], its components at the sphere of influence can be defined from the interplanetary orbital parameters (a, e, i), semi-major axis, eccentricity and inclination

[1] Apophis is a near Earth asteroid upon which many studies were carried out in the last two decades, since at the first monitoring it appeared, to be later denied, impacting with Earth at its close approach.

respectively, the Tisserand parameter T and the two angles (θ, φ) characterising the incoming asymptote of the hyperbolic close encounter.

2.2 B-plane visualisation tool

The b-plane reference frame is a cartesian reference frame centred at the current planet centre of mass, with axes $(\hat{\xi}, \hat{\eta}, \hat{\zeta})$, whose components, denoting with $\boldsymbol{v}_p$ the planet's velocity, in the planetocentric reference frame can be defined as [6]:

$$\hat{\eta} = \frac{\boldsymbol{U}}{\|\boldsymbol{U}\|}; \quad \hat{\xi} = \frac{\boldsymbol{U} \times \boldsymbol{v}_p}{\|\boldsymbol{U} \times \boldsymbol{v}_p\|}; \quad \hat{\zeta} = \hat{\xi} \times \hat{\eta}. \tag{2.1}$$

A generic point $\boldsymbol{x}_{cartesian}$ in the planetocentric reference frame can then be expressed in the b-plane reference frame simply by performing

$$\boldsymbol{x}_{b-plane} = \begin{Bmatrix} \xi \\ \eta \\ \zeta \end{Bmatrix} = \left[\hat{\xi}, \hat{\eta}, \hat{\zeta}\right]^T \boldsymbol{x}_{cartesian}. \tag{2.2}$$

Each coordinate in the b-plane representation [7] expresses a remarkable property of the current close approach: ξ describes the minimum distance between the two interplanetary orbits, ζ the time shift with respect to the close approach to happen at the minimum distance, η the distance from the pericentre of the hyperbolic planetocentric trajectory. With b being the impact parameter it holds then that [8]:

$$\xi^2 + \zeta^2 = b^2 \tag{2.3}$$

2.3 Resonant circles

A given resonance is identified by a certain post encounter semi-major axis a_0' ([4]), so that after a time defined either as k small body interplanetary orbits or h planet orbits the two bodies feature again a close encounter at the same position of the first one. a_0' can then be defined as:

$$a_0' = \left(\frac{k}{h}\right)^{2/3}. \tag{2.4}$$

The outgoing asymptote for this resonance condition features an angle θ_0' defined as ([4]):

$$cos\, \theta_0' = \frac{1 - 1/a_0' - U^2}{2U} \tag{2.5}$$

and a given resonant condition can be represented in the b-plane by a circle centred on the $\hat{\zeta}$ axis at $\zeta = D$ and with radius R [4]:

$$\xi^2 + \zeta^2 - 2D\zeta + D^2 = R^2 \tag{2.6}$$

where, with m to denote the mass of the planet expressed in Sun masses [4], the quantities involved are defined as:

$$D = \frac{2c^* \sin\theta}{\cos\theta_0' - \cos\theta}; \quad R = \left|\frac{c^* \sin\theta_0'}{\cos\theta_0' - \cos\theta}\right|; \quad c^* = \frac{m}{U^2}; \quad \cos\theta = \frac{U_y}{U}. \tag{2.7}$$

3 RESONANT BELTS – ANALYTICAL FORMULATION

As defined in Section (2.3) the quantity a_0' models perfectly phased resonances only, i.e. any consequent close encounter not happening exactly after integer multiples of the orbital periods would not be treated as resonant return. To apply this formalism to the study of actual closely approaching bodies it may be worth to extend this definition to include also non-perfectly phased close encounters as resonant ones.

3.1 Quasi-resonance definition

The definition of quasi-resonance can be arbitrary, based on what time interval one wants to consider as identifying an actual resonance. A mathematical definition may be found by looking first at what cases need to be classified as such [9], obtaining the relative deviation $\Delta_{k/h}$ from the perfect resonance $(k/h)_j$ as

$$\Delta_{k/h} = \frac{\frac{t_{object}}{t_{planet}} - \left(\frac{k}{h}\right)_j}{\left(\frac{k}{h}\right)_j} \tag{3.1}$$

with t to denote the generic orbital period and classifying an object as resonant whether the quasi-resonance condition $\left|\Delta_{k/h}\right| \leq \tilde{\Delta}$ is satisfied, with $\tilde{\Delta}$ directly dependent on the time interval mentioned above.

Equation (3.1) can then be conceptually reverted, imposing $\left|\Delta_{k/h}\right| = \tilde{\Delta}$ to define two boundary ratios $(k/h)^{\pm}_{quasi-j}$, upper and lower respectively, associated with the perfect resonant configuration $(k/h)_j$:

$$\left(\frac{k}{h}\right)^{\pm}_{quasi-j} = \left(\frac{k}{h}\right)_j \left(1 \pm \tilde{\Delta}\right). \tag{3.2}$$

3.2 Resonant belts

Looking back to Equation (2.4) one can observe that the ratio (k/h) is directly linked to the resonant circle parameters, it is then straight forward to say that each of the two ratios from Equation (3.2) identifies a new circle, and the two together bound the *resonant belt*, the locus of the points in the b-plane satisfying the quasi-resonance condition.

4 NUMERICAL PROPAGATIONS

Each sample in the Monte Carlo Simulation has been propagated by accounting for the gravitational forces coming from all the planets in the Solar System and general relativity effects.

4.1 General relativity model

General Relativity effects in the N-Body problem can be described by the following equation [10] centred at the Solar System barycentre:

$$\ddot{\boldsymbol{r}}_\iota = \sum_{j\neq i} \frac{\mu_j(\boldsymbol{r}_j - \boldsymbol{r}_i)}{r_{ij}^3}\Bigg\{1 - \frac{4}{c^2}\sum_{k\neq i}\frac{\mu_k}{r_{ik}} - \frac{1}{c^2}\sum_{k\neq j}\frac{\mu_k}{r_{jk}} + \left(\frac{v_i}{c}\right)^2 + 2\left(\frac{v_j}{c}\right)^2 - \frac{4}{c^2}\dot{\boldsymbol{r}}_\iota\cdot\dot{\boldsymbol{r}}_J - \frac{3}{2c^2}\left[\frac{(\boldsymbol{r}_i - \boldsymbol{r}_j)\cdot\dot{\boldsymbol{r}}_J}{r_{ij}}\right]^2 + \frac{1}{c^2}\sum_{j\neq i}\frac{\mu_j}{r_{ij}^3}\{[\boldsymbol{r}_i - \boldsymbol{r}_j]\cdot[4\dot{\boldsymbol{r}}_\iota - 3\dot{\boldsymbol{r}}_J]\}(\dot{\boldsymbol{r}}_\iota - \dot{\boldsymbol{r}}_J)\Bigg\} + \frac{1}{2c^2}\sum_{j\neq i}\frac{\mu_j(\boldsymbol{r}_j - \boldsymbol{r}_i)}{r_{ij}^3}\left((\boldsymbol{r}_j - \boldsymbol{r}_i)\cdot\ddot{\boldsymbol{r}}_J\right) + \frac{7}{2c^2}\sum_{j\neq i}\frac{\mu_j\ddot{\boldsymbol{r}}_J}{r_{ij}} \tag{4.1}$$

where each subscript $(i, j, k) = 1, \dots, N$ denotes a generic one of the N massive bodies and their current state with respect to the centre of the reference frame, μ identifies the gravitational parameter and c stands for the speed of light in vacuum. All the bold quantities in Equation (4.1) are to be meant as 3×1 vectors and the other scalar terms are defined as $r_{ij} = \|\boldsymbol{r}_i - \boldsymbol{r}_j\|$ and $v_i = \|\dot{\boldsymbol{r}}_\iota\|$. One can note that the acceleration[2] of body i ($\ddot{\boldsymbol{r}}_\iota$) linearly depends on the acceleration of body j ($\ddot{\boldsymbol{r}}_J$), hence Equation (4.1) can be adapted to obtain the acceleration of all the N bodies at each time iteration of the numerical propagation by simply solving the augmented linear system

$$(I_{3N\times 3N} - R)\ddot{\boldsymbol{r}}_{aug} = \boldsymbol{a}_{aug}. \tag{4.2}$$

It is worth to mention that this manipulation relies entirely on the need to implement the dynamics with its state-space formulation. No further assumption or approximation has been made (the method can then be used for the most general N-body propagation), the quantity $\ddot{\boldsymbol{r}}_{aug}$ is simply the sorted collection in a $3N \times 1$ column vector of all the accelerations $\ddot{\boldsymbol{r}}_\iota$ of the N bodies, whereas all the other quantities involved depend on the state only: $\boldsymbol{a}_{aug}$ is again a $3N \times 1$ column vector collecting all the terms on the right hand side of Equation (4.1) which do not get multiplied by $\ddot{\boldsymbol{r}}_J$, R is a $3N \times 3N$ matrix collecting all the state dependant elements acting as linear coefficients on $\ddot{\boldsymbol{r}}_J$ and $I_{3N\times 3N}$ denotes the $3N \times 3N$ identity matrix. Note that there is no strict rule on how to sort such elements, any collection consistent among $\ddot{\boldsymbol{r}}_{aug}$, $\boldsymbol{a}_{aug}$ and R will produce the correct N-body accelerations sorted in the same way.

By finally assuming the small object to not affect the motion of the N-bodies, its acceleration can be obtained by solving Equation (4.1) plugging in the N-body accelerations coming from the solution of Equation (4.2).

This briefly mentioned method has already successfully passed the validation process, where integrations 100 years forward in time feature a relatively low computational cost, with results basically identical, uncertainties propagation aside, to NASA's ephemerides data for all the test cases analysed.

[2] In the current notation the symbol $\dot{x}$ identifies the first time derivative of x, thus $\ddot{x}$ denotes the second time derivative.

4.2 Propagation and Monte Carlo settings

Apophis' nominal orbital motion was propagated at the turn of the predicted fly-by of Earth happening on 2029, thirty years forward in time. 2000 samples with symmetric gaussian distribution have been generated from the nominal initial condition (obtained from ephemerides data, available in Table 1) by deviating each element of the initial position and velocity vectors of a relative quantity x, with $-0.005\% \leq x \leq 0.005\%$.

Epoch	r_x	r_y	r_z	v_x	v_y	v_z
[MJD2000]	$[km]$	$[km]$	$[km]$	$[km/s]$	$[km/s]$	$[km/s]$
10227	17432973	132874235	49787825	-28.38275	8.74813	2.53606

Table 1: Initial epoch, position and velocity of the nominal configuration, in a cartesian equatorial reference frame centred in the Solar System's barycentre.

The propagator integrates the N-body dynamics (Sun, Moon and all the planets in the Solar System) and accounts for General Relativity as perturbing effect. The states of the N-bodies are introduced by embedding SPICE toolkit and the related kernel data as databases.

5 RESONANT BELTS – RESULTS AND NUMERICAL VALIDATION PROCESS

Resonant circles and belts for Apophis' nominal configuration are plotted in the b-plane at the entrance of Earth's sphere of influence. Note that the circle parameters D and R depend (Equations (2.4), (2.5) and (2.7)) on the body's planetocentric velocity $\boldsymbol{U}$ and the mass of Earth m, thus it is possible to obtain such quantities just from the first propagation step inside the sphere of influence.

In this work the quasi-resonance parameter $\widetilde{\Delta}$ is defined as in [9], i.e. $\widetilde{\Delta} = 0.005$. Note that this value represents both the quasi-resonance threshold for the numerical simulations and the parameter used to draw the resonant belts.

5.1 From resonant circles to resonant belts

The analytical resonant circles [4] and the derived belts are plotted in Figure 1.

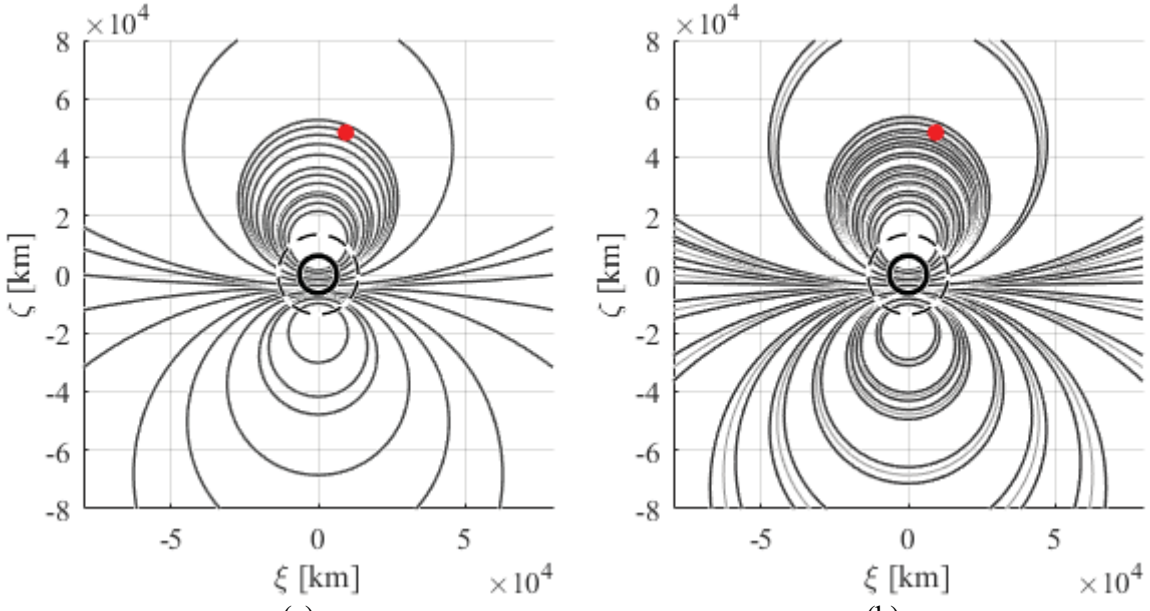

(a) (b)

Figure 1: The resonant circles in (a) are now extended to resonant belts as in (b), according to the definitions presented in Section (3).

As expected, a belt-shaped locus of points bounded by the two newly defined circles is obtained, with the original perfect resonant circle included within the same.

5.2 Comparison with simulated resonant belts

The validation process is initiated by comparing the analytical resonant belts with the simulated resonances. All the samples of the Monte Carlo simulation have passed through the quasi-resonance condition check, to then be plotted together with the resonant belts in the b-plane representation reported in Figure 1.

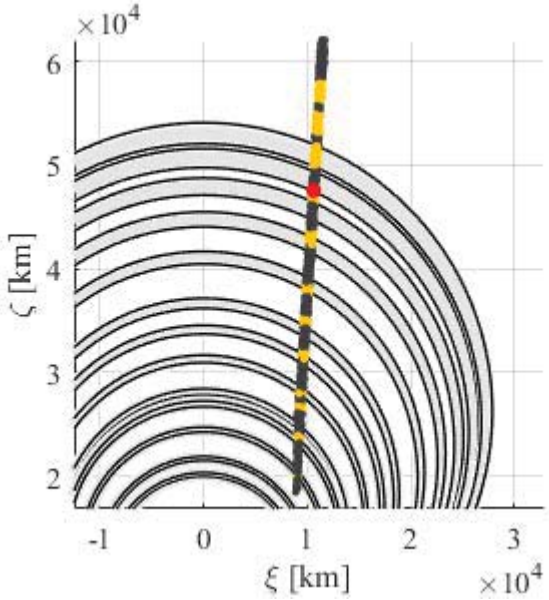

Figure 2: The analytical resonant belts are bounded by the black lines and are identified by the light grey area, whereas the sample properties are classified according to three different colours (the yellow points satisfy the quasi-resonant condition, the dark grey ones are simple close approaches and the red point identifies the reference body for the current b-plane).

A sort of regular deviation is observed, with the simulated belts to follow the sequence of the analytical ones but being shifted in the positive ζ axis direction.

6 EXPERIMENTAL IMPROVEMENTS AND FUTURE ANALYTICAL DEVELOPMENTS

Despite the simulated and the analytical belts do not coincide, the regular shift experienced (Figure 2) suggests that there still must be a way to model such a phenomenon. Two experimental solution have been found, to be presented in the upcoming sections (6.1) and (6.2). Finally, a possible development direction is explored in Subsection (6.3).

6.1 Quadratic shift experimental law: elliptical resonant belts

Given a certain resonant circle, the shift from the simulated belt can be modelled as a quadratic experimental variation law of the radius of the circle itself:

$$\xi^2 + \zeta^2 - 2D\zeta + D^2 = R^2 + c_1 + c_2\zeta + c_3\zeta^2. \tag{6.1}$$

The three coefficients (c_1, c_2, c_3) may be found by imposing three experimentally variated circles to pass through three correspondent[3] simulated belts. Once those coefficients are determined, with some algebraic manipulation Equation (6.1) can be manipulated to obtain the canonical equation of an ellipse centred on the ζ axis, of the form:

$$\frac{\xi^2}{A^2} + \frac{(\zeta - C)^2}{B^2} = 1. \tag{6.2}$$

with the two semi-axes (A, B) and the ζ coordinate of the centre C to directly depend on the original circle parameters (D, R) and the coefficients (c_1, c_2, c_3) through simple algebraic relations. New elliptical resonant belts are obtained starting from the previous circular resonant belts, with all of them featuring a dependence on the same coefficients (c_1, c_2, c_3), which have been obtained by imposing the analytical-numerical correspondence of top, bottom and central belts. The new resonant belts are plotted in Figure 3, according to the same colour convention and b-plane representation of Figure 2.

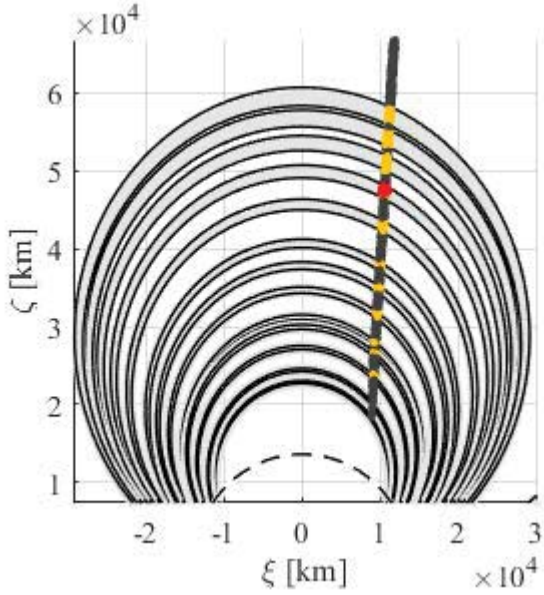

Figure 3: All the simulated and analytical resonant belts now perfectly coincide. Despite being just experimental, this regular law suggests that, at least for the Apophis' case, there may be a physically based analytical formulation of the elliptical resonant belts.

6.2 Experimental cancellation of rigid shift

Within this second experimental approach the rigid part of the shift visible on the plot in Figure 2 has been cancelled by considering, instead of the first numerical step immediately inside Earth's sphere of influence, the step of the planetocentric ingoing trajectory which led to the perfect correspondence of the resonant belt associated with the reference point. The same b-plane analysis is performed in Figure 4, together with a new model of elliptical resonant belts with the same shape of what studied in Subsection (6.1), but with the coefficients (c_1, c_2, c_3) computed for the new cloud of b-plane points.

[3] The correspondence may be easily found by looking at the regular behaviour of the belts, e.g. the top analytical belt must correspond to the top simulated one.

6.3 Suggested future analytical developments

The experimental results presented in Subsections (6.1) and (6.2) allow to make some considerations about what possible physical phenomena could be introducing such a shift between simulated and analytical belts.

6.3.1 N-body and 2-body propagation related

Since the expression of the resonant circles [4] has been obtained with a patched conics 2-body planetocentric model, the rigid part of the shift may be due to the N-body nature of the numerical propagation carried out even inside Earth's sphere of influence. The first integration step inside the sphere of influence of this close approach analysis may be still experiencing small perturbing effects due to mainly the Sun, but slightly deviating the trajectory from the one predicted by a 2-body model.

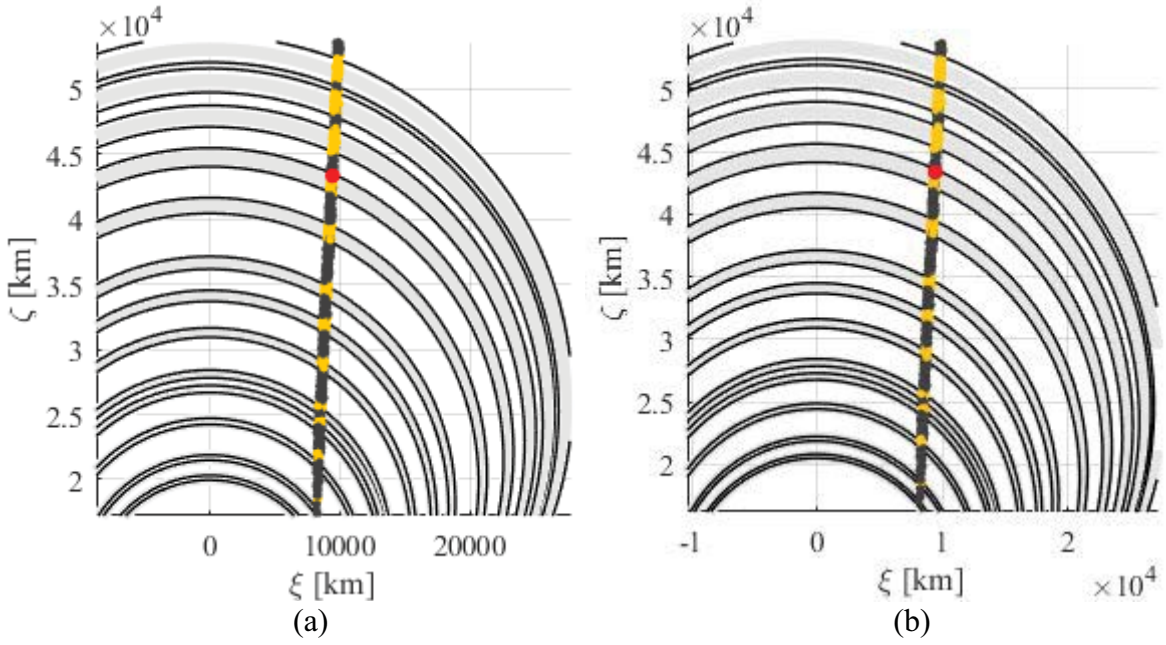

Figure 4: The circular resonant belts in (a) are now much closer to the simulated resonances than in Figure (2), nevertheless, with respect to the reference point, the furthest elements of the simulated cloud are observed to experience a increasing shift. The elliptical belts are plotted in (b), even in this case the elliptical shape seems to be perfectly matching the simulated resonances.

A possible step towards a complete handling of this physical phenomenon may be either modelling the missing dynamics in the analytical formulation of the resonant belts or identifying another time step of analysis, where the 2-body almost perfectly approximates the complete dynamics and which, however, must provide results as reliable as the full simulation.

An improved analytical model may be to find the actual deflection by considering the most relevant missing effects in the Sun-Planet-Small Body system first. The patched conics method approximates the planet's motion, when the small body is inside the sphere of influence of the same, as a straight line, whereas the planet's velocity vector rotates of a few degrees during the close approach occurrence (for example, approximating Earth's motion with a circular orbit and with a fly-by total duration of 48h, Earth's velocity vector would rotate 1.97° counter-clockwise in the orbital plane). Such an effect is legitimately enhanced for relatively slow fly-bys and close approaches of the inner planets, where smaller times provide larger planet's velocity rotations than the outer ones.

6.3.2 Radius' small linear velocity perturbations

The results presented in Figure 4 (b) show that, even after the experimental cancellation of the rigid part, the shift increases the further the points get from the reference. Such a phenomenon may be the nature of the analysis itself, given that it involves the actual simulations with their true resonances and the analytical resonant belts of the reference sample only. Note that, from Equations (2.1) and (2.2) [6], each sample features its own close encounter time and planetocentric velocity, factors that make both the b-plane axes and its correspondent resonant belts unique and different than the reference's ones.

A possible approach to model the difference in planetocentric velocity is the study of the effect of small linear perturbations on the radius[4] of each bound. Figure 5 represents the square of the radius of the reference perfect resonant circle as function of the planetocentric velocity, which seems to be smooth enough to expect accurate results whether an approximation of this kind is performed.

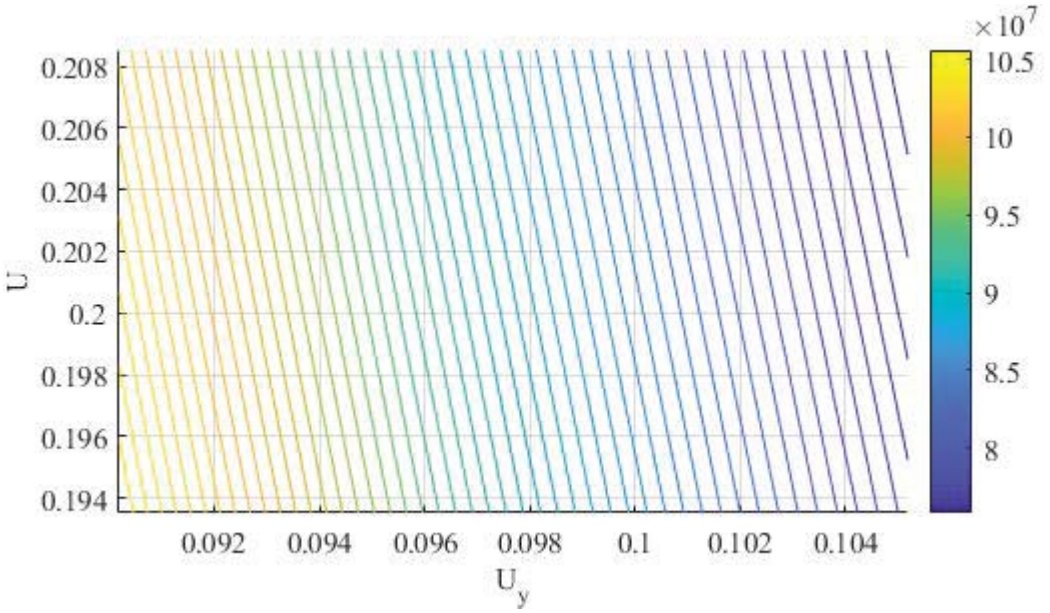

Figure 5: Square of the radius of the perfect resonant circle associated with the reference point. The axes of magnitude and y component of the planetocentric velocity range from the minimum to the maximum one among all the elements of the cloud.

Note however that the elliptical shape of the resonant belts arose from a quadratic variation law over ζ, thus a proper mathematical link between the linear velocity perturbation and a law as such would be needed as well.

7 CONCLUSION AND OUTLOOK

A first step to adapt the already available orbital resonance theory to the study of a cloud of bodies all in the same b-plane representation has been made, particularly by extending the concept of resonant circle to the one of resonant belt, associated with a more applicable definition of resonance in the context of planetary protection and defence.

Despite the physical phenomena hidden beneath the simulated resonances, an elliptical re-formulation of the circular belts was experimentally proven to be an accurate mathematical model, at least under the analysed ranges of velocities and b-plane coordinates. Such a formulation extends and includes the 2-body and single point case upon which the whole

[4] Note that, as in all the definitions in Equation (2.7) and once fixed the resonance, the only variables characterising each resonant circle are the planetocentric velocity magnitude and the y component.

resonance theory was built. In this last case the results of an experimental variation as the one presented would naturally provide the initial resonant circles.

The regularity and the accuracy of the experimental law modelled suggests that an analytical derivation of the elliptical resonant belts may be possible, including in the analysis the N-body dynamics related effects and the different properties of the points composing the cloud. The formulation of a robust resonance model as such may be eventually used for the detection of possible resonances, reducing the computational effort that would be needed whether the full dynamics is simulated, but still obtaining accurate analytical predictions.

8 ACKNOWLEDGMENTS

The research leading to these results has received funding from the European Research Council (ERC) under the European Union's Horizon 2020 research and innovation programme as part of project COMPASS (Grant agreement No 679086) www.compass.polimi.it.

REFERENCES

[1] G. Kminek, "ESA planetary protection requirements, Technical Report ESSB-ST-U-001," 2012.
[2] Y. zhong Luo and Z. Yang, "A review of uncertainty propagation in orbital mechanics," *Progress in Aerospace Sciences*. 2017.
[3] C. H. Acton, "Ancillary data services of NASA's navigation and Ancillary Information Facility," *Planet. Space Sci.*, 1996.
[4] G. B. Valsecchi, A. Milani, G. F. Gronchi, and S. R. Chesley, "Resonant returns to close approaches: Analytical theory," *Astron. Astrophys.*, 2003.
[5] A. Carusi, G. B. Valsechi, and R. Greenberg, "Planetary close encounters: geometry of approach and post-encounter orbital parameters," *Celest. Mech. Dyn. Astron.*, 1990.
[6] E. J. Opik, "Interplanetary Encounters: Close-Range Gravitational Interactions," vol. 2, 1976.
[7] A. Bourdoux and D. Izzo, "Characterization and hazard mitigation of resonant returning Near Earth Objects," 2005.
[8] A. Milani, S. R. Chesley, P. W. Chodas, and G. B. Valsecchi, "Asteroid Close Approaches: Analysis and Potential Impact Detection," *Asteroids III*, 2002.
[9] C. Colombo, F. Letizia, and J. Van Der Eynde, "SNAPPshot ESA planetary protection compliance verification software Final report, Technical Report ESA-IPL-POM-MB-LE-2015-315," 2016.
[10] P. K. Seidelmann, *Explanatory Supplement To The Astronomical Almanac*. 20 Edgehill Road, Mill Valley, CA, 94941: University Science Books.